Analytical forces for the optimized effective potential calculations

Chen Huang*

Department of Scientific Computing, Materials Science and Engineering Program, National High Magnetic Field Laboratory, Florida State University, Tallahassee, Florida 32306, USA

E-mail: chuang3@fsu.edu

Abstract

The optimized effective potential (OEP) equation is an ill-conditioned linear system when using finite basis sets. Without any special treatment, the obtained exchangecorrelation (XC) potential may have unphysical oscillations. One way to alleviate this problem is to regularize the solutions; however, a regularized XC potential is not the exact solution to the OEP equation. As a result, the system's energy is no longer variational against the Kohn-Sham (KS) potential, and the analytical forces cannot be derived from the Hellmann-Feynman theorem. In this work, we develop a robust and nearly black-box OEP method to ensure that the system's energy is variational against the KS potential. The basic idea is to add a penalty function that regularizes the XC potential to the energy functional. Analytical forces can then be derived based on the Hellmann-Feynman theorem. Another key result is that the impact of the regularization can be much reduced by regularizing the difference between the XC potential and an approximate XC potential, rather than regularizing the XC potential. Numerical tests show that forces and the energy differences between systems are not sensitive to the regularization coefficient, which indicates that in practice accurate structural and electronic properties can be obtained without extrapolating the regularization coefficient

to zero. We expect this new method to be found useful for calculations that employ advanced, orbital-based functionals, especially for these applications that require efficient force calculations.

1 Introduction

The accuracy of Kohn-Sham density functional theory (KS-DFT)^{1,2} depends on the accuracy of the exchange-correlation (XC) energy functional. Advanced XC functionals that depend on the KS orbitals were actively developed in the past.³ For example, the correlation energy functional based on the random-phase approximation (RPA) shows good results for the α - γ phase transition pressure of cerium,⁴ the bulk properties of solids,⁵ van der Waals energy between graphene and metals,⁶ and CO's adsorption energies on transition metals.⁷

For orbital-dependent functionals, their XC potential can be obtained by solving the optimized effective potential (OEP) equation.^{3,8–11} Unfortunately, the OEP equation is an ill-conditioned linear system when finite basis sets are used.^{12,13} As a result, the obtained XC potential can contain unphysical oscillations in real space. Note that the OEP equation can be avoided, if we directly minimize the total energy against the KS potential.¹⁴ Based on this idea, analytical forces have been derived for the exact exchange.¹⁵ However, in practice KS-DFT is usually solved by an efficient iterative scheme, ¹⁶ which requires solving the OEP equation. Therefore, in this work we stick with the iterative scheme and focus on solving the OEP equation.

Various methods have been developed in the past to solve the OEP equation. One group of methods solve the equation approximately, such as the Krieger-Li-Iafrate approximation, ¹⁷ the common energy denominator approximation, ¹⁸ the localized Hartree-Fock method, ¹⁹ and the effective local potential method. ²⁰ Some other methods solve the OEP equation by tackling the singularity of the KS linear response. Hirata et al. removed the singularity by projecting the OEP equation into the space spanned by the vectors that are not in the null space of the KS linear response. ^{12,13} With properly constructed basis functions, the OEP

equation has been solved for the exact exchange ^{21,22} and the RPA correlation, ^{23,24} and the corresponding analytical forces were derived. ^{22,24}

A more black-box method for solving the OEP equation was developed by Yang and coworkers, ^{25,26} in which the unphysical oscillations are suppressed using the regularization technique. The drawback is that the regularized XC potential is no longer the exact solution to the OEP equation. Thus, the system's energy is not variational against the KS potential, and analytical forces cannot be derived from the Hellmann-Feynman theorem. Without efficient force calculations, many important tasks, such as structure optimization, molecular dynamics, and vibrational frequency calculations, become time-consuming.

The goal of this work is to develop a new OEP method that allows for deriving analytical forces based on the Hellmann-Feynman theorem. The basic idea is to add a penalty function that regularizes the XC potential to the energy. The OEP equation derived from this modified energy is automatically regularized. Since the modified energy is variational to the KS potential, analytical forces can be derived from the Hellmann-Feynman theorem. Another goal of this work is to reduce the impact of the penalty function on DFT calculations. Different from our previous work that regularized the XC potential itself, ²⁷ here we regularize the difference between the XC potential and an approximate XC potential. This greatly reduces the impact of regularization on DFT calculations.

The paper is organized as follows. In Section 2, we introduce a new regularization scheme that regularizes the difference between an XC potential and an approximate XC potential. The magnitude of the regularization is controlled by the regularization coefficient λ . To extrapolate the energies to $\lambda = 0$, we derive the asymptotic behavior of the energies for $\lambda \to 0$. We then derive the regularized OEP equation and the analytical forces. In Section 4, we first examine the convergence speed of the new OEP method and then demonstrate the extrapolation of the energies to $\lambda = 0$. We show that, with the same λ , the new regularization scheme produces much less error than the old scheme. We then validate the analytical forces and show that the forces are not sensitive to λ . In the end, we focus on the energy difference

calculations and demonstrate that the energy differences are also not very sensitive to λ .

2 Theoretical methods

2.1 Regularize the XC potential

The total energy of KS-DFT is defined as

$$E_{KS} = T_s + E_{xc} + J + E_{ext} - TS \tag{1}$$

where T_s is the KS kinetic energy, E_{xc} is XC energy, J is the Hartree energy, E_{ext} is the external energy, T is the electronic temperature, and S is the electronic entropy. The occupation numbers of the KS orbitals are assigned according to the Fermi-Dirac distribution. To regularize the XC potential, we recently introduced a regularization term E_p to the total energy.²⁷ The modified total energy is

$$E = E_{KS} + \lambda E_p \tag{2}$$

with

$$E_p = \sum_{\sigma} \frac{1}{4} \int |\nabla [v_{s,\sigma}(\vec{r}) - v_H(\vec{r}) - v_{ext}(\vec{r})]|^2 dr^3$$
 (3)

where σ is the spin index. $v_{s,\sigma}$ and v_H are the KS and Hartree potentials, respectively. E_p is defined based on the observation that at the convergence $v_{s,\sigma} - v_H - v_{ext}$ is equal to the sum of the XC potential $v_{xc,\sigma}$ and the regularization potential $v_{p,\sigma} = \delta E_p/\delta \rho_{\sigma}$. The OEP equation derived based on the modified energy E is regularized, so that the physical solutions can be obtained.²⁷ In addition, the modified energy E is variational against the KS potential, and analytical forces can be derived.²⁷

A key result of this work is that the impact of E_p on DFT calculations can be significantly reduced by only regularizing the difference between $(v_{xc} + v_p)$ and an approximate XC potential. In this work, Perdew-Wang local density approximation ²⁸ (LDA) XC potential $v_{xc}^{\rm LDA}$ is used as the approximate XC potential. The new definition for E_p is

$$E_p = \sum_{\sigma} \frac{1}{4} \int |\nabla [v_{s,\sigma}(\vec{r}) - v_H(\vec{r}) - v_{ext}(\vec{r}) - v_{xc,\sigma}^{LDA}(\vec{r})]|^2 dr^3.$$
 (4)

Since v_p is much smaller than v_{xc} in practice, equation 4 mainly regularize the difference between v_{xc} and v_{xc}^{LDA} . In this work, all the results are calculated using the new regularization (Eq. 4), unless explicitly specified. To simplify future discussions, let's define

$$u_{\sigma}(\vec{r}) = v_{s,\sigma}(\vec{r}) - v_{ext}(\vec{r}) - v_H(\vec{r}) - v_{xc,\sigma}^{LDA}(\vec{r}), \tag{5}$$

and Eq. 4 becomes

$$E_p = \frac{1}{4} \sum_{\sigma} \int |\nabla u_{\sigma}(\vec{r})|^2 dr^3. \tag{6}$$

Similarly, the total energy can be re-organized as

$$E = T_s + E_{rc}^{LDA} + J + E_{ext} - TS + (E_{xc} - E_{rc}^{LDA} + \lambda E_p), \tag{7}$$

in which the terms in the parenthesis are now treated as a correction to the KS-DFT-LDA energy. The potential due to these terms is

$$v_{\text{xcp},\sigma}(\vec{r}) = \frac{\delta(E_{xc} - E_{xc}^{\text{LDA}} + \lambda E_p)}{\delta \rho_{\sigma}(\vec{r})},$$
(8)

which is obtained by solving the OEP equation discussed later.

2.2 Estimate the total energy at $\lambda = 0$

The total energy E defined by Eq. 2 is a function of λ . To estimate E at $\lambda = 0$, we derive its first-order correction. The gradient of E with respect to λ is

$$\frac{dE}{d\lambda} = \sum_{\sigma} \int \frac{\delta E}{\delta v_{s,\sigma}(\vec{r})} \frac{dv_{s,\sigma}(\vec{r})}{d\lambda} dr^3 + \frac{\partial E}{\partial \lambda} = E_p, \tag{9}$$

in which we have used the fact that $\delta E/\delta v_{s,\sigma} = 0$ at convergence. The first-order corrected energy E_1 is obtained as

$$E_1 = E - \lambda E_p = E_{KS},\tag{10}$$

which means that we can just take E_{KS} as the first-order corrected energy at the end of the calculations. In this work, energy-related quantities, such as energy differences and bulk modulus, are all calculated using E_{KS} unless explicitly specified.

To obtain a more accurate estimation of E at $\lambda = 0$, next we derive a formula for extrapolating the energies to $\lambda = 0$. Note that E_p , which measures the fluctuation of the XC potentials, diverges as $\lambda \to 0$. Let's denote its asymptotic behavior as $E_p(\lambda) \approx c\lambda^{-\alpha}$ with $0 < \alpha < 1$ and c being an unknown constant. The reason for $\alpha < 1$ is that λE_p is expected to be zero at $\lambda = 0$. With Eq. 9, we have

$$\frac{dE}{d\lambda} = E_p \approx c\lambda^{-\alpha}.\tag{11}$$

Integrating Eq. 11, we obtain the asymptotic behavior of E_{λ} for $\lambda \to 0$

$$E = E_0 + \frac{c}{1 - \alpha} \lambda^{1 - \alpha},\tag{12}$$

where E_0 denotes the energy at $\lambda = 0$. The asymptotic behavior of E_{KS} can be derived based on Eq. 12 as

$$E_{KS} = E - \lambda E_p = E_0 + \frac{c\alpha}{1 - \alpha} \lambda^{1 - \alpha}, \tag{13}$$

Eqs. 12 and 13 are used to extrapolate E and E_{KS} to $\lambda = 0$ in this work for obtaining the benchmarks.

2.3 The OEP equation

The derivation of the OEP equation follows the similar idea as in our previous work,²⁷ but with the new definition of E_p from Eq. 6. The OEP equation is

$$\frac{\delta(E_{xc} - E_{xc}^{\text{LDA}} + \lambda E_p)}{\delta v_{s,\sigma}(\vec{r})} = \sum_{\sigma'} \int v_{\text{xcp},\sigma'}(\vec{r}_1) \frac{\rho_{\sigma'}(\vec{r}_1)}{\delta v_{s,\sigma}(\vec{r})} dr_1^3, \tag{14}$$

which can be written compactly in the matrix representation as

$$\begin{bmatrix}
\frac{\delta(E_{xc} - E_{xc}^{\text{LDA}} + \lambda E_p)}{\delta v_{s,\alpha}} \\
\frac{\delta(E_{xc} - E_{xc}^{\text{LDA}} + \lambda E_p)}{\delta v_{s,\beta}}
\end{bmatrix} = \begin{bmatrix}
X_{\alpha\alpha} & X_{\alpha\beta} \\
X_{\beta\alpha} & X_{\beta\beta}
\end{bmatrix} \begin{bmatrix}
v_{\text{xcp},\alpha} \\
v_{\text{xcp},\beta}
\end{bmatrix}.$$
(15)

 $X_{\sigma\sigma'} = \delta\rho_{\sigma}/\delta v_{s,\sigma'}$ is the KS linear response. In this work, a modified Heyd-Scuseria-Ernzerhof (HSE) functional^{29–32} is used for E_{xc} (see Appendix A for details). The derivations of $\delta E_{xc}/\delta v_{s,\sigma}$ and $\delta E_{xc}^{\text{LDA}}/\delta v_{s,\sigma}$ are given in Appendix B.

In what follows, we derive $\delta E_p/\delta v_{s,\sigma}$. For the spin α , we have

$$\frac{\delta E_p}{\delta v_{s,\alpha}(\vec{r})} = \sum_{\sigma} \int \frac{\delta E_p}{\delta u_{\sigma}(\vec{r}_1)} \frac{\delta u_{\sigma}(\vec{r}_1)}{v_{s,\alpha}(\vec{r})} dr_1^3.$$
 (16)

Based on u_{σ} 's definition in Eq. 5, in the matrix representation, we have

$$\frac{\delta u_{\alpha}}{\delta v_{s,\alpha}} = I - K_H (X_{\alpha\alpha} + X_{\beta\alpha}) - K_{\alpha\alpha}^{\text{LDA}} X_{\alpha\alpha} - K_{\alpha\beta}^{\text{LDA}} X_{\beta\alpha}$$
 (17)

$$\frac{\delta u_{\beta}}{\delta v_{s,\alpha}} = -K_H (X_{\alpha\alpha} + X_{\beta\alpha}) - K_{\beta\beta}^{\text{LDA}} X_{\beta\alpha} - K_{\beta\alpha}^{\text{LDA}} X_{\alpha\alpha}$$
 (18)

where $K_H(\vec{r}_1, \vec{r}_2) = 1/|\vec{r}_1 - \vec{r}_2|$ is the kernel of the Hartree energy and $K_{\sigma'\sigma}^{\text{LDA}}$ is the kernel of the LDA XC energy $K_{\sigma\sigma'}^{\text{LDA}}(\vec{r}_1, \vec{r}_2) = \delta^2 E_{xc}^{\text{LDA}}/\delta \rho_{\sigma}(\vec{r}_1) \delta \rho_{\sigma'}(\vec{r}_2)$. Insert Eqs. 17 and 18 into

Eq. 16 and note $\delta E_p/\delta u_{\sigma}=-\frac{1}{2}\nabla^2 u_{\sigma}$, we obtain

$$\frac{\delta E_p}{\delta v_{s,\alpha}} = -\frac{1}{2} [I - (X_{\alpha\alpha} + X_{\alpha\beta}) K_H - X_{\alpha\alpha} K_{\alpha\alpha}^{\text{LDA}} - X_{\alpha\beta} K_{\beta\alpha}^{\text{LDA}}] \nabla^2 u_{\alpha}
-\frac{1}{2} [-(X_{\alpha\alpha} + X_{\alpha\beta}) K_H - X_{\alpha\beta} K_{\beta\beta}^{\text{LDA}} - X_{\alpha\alpha} K_{\alpha\beta}^{\text{LDA}}] \nabla^2 u_{\beta}.$$
(19)

Similarly, for the spin β we have

$$\frac{\delta E_p}{\delta v_{s,\beta}} = -\frac{1}{2} [I - (X_{\beta\beta} + X_{\beta\alpha}) K_H - X_{\beta\beta} K_{\beta\beta}^{\text{LDA}} - X_{\beta\alpha} K_{\alpha\beta}^{\text{LDA}}] \nabla^2 u_{\beta}
-\frac{1}{2} [-(X_{\beta\beta} + X_{\beta\alpha}) K_H - X_{\beta\alpha} K_{\alpha\alpha}^{\text{LDA}} - X_{\beta\beta} K_{\beta\alpha}^{\text{LDA}}] \nabla^2 u_{\alpha}.$$
(20)

To simplify the derivations, we re-write Eqs. 19 and 20 as

$$\frac{\delta E_p}{\delta v_{s,\alpha}} = t_\alpha - \frac{1}{2} \nabla^2 u_\alpha \tag{21}$$

$$\frac{\delta E_p}{\delta v_{s,\beta}} = t_\beta - \frac{1}{2} \nabla^2 u_\beta. \tag{22}$$

where t_{α} and t_{β} contains all the terms on the right-hand side of Eqs. 19 and 20, except the terms involving the identity matrices, and are

$$\begin{bmatrix} t_{\alpha} \\ t_{\beta} \end{bmatrix} = \frac{1}{2} \begin{bmatrix} X_{\alpha\alpha} & X_{\alpha\beta} \\ X_{\beta\alpha} & X_{\beta\beta} \end{bmatrix} \begin{bmatrix} v_1 \\ v_2 \end{bmatrix}$$
 (23)

with

$$v_1 = (K_H + K_{\alpha\alpha}^{\text{LDA}}) \nabla^2 u_\alpha + (K_H + K_{\alpha\beta}^{\text{LDA}}) \nabla^2 u_\beta$$
 (24)

$$v_2 = (K_H + K_{\beta\alpha}^{\text{LDA}}) \nabla^2 u_\alpha + (K_H + K_{\beta\beta}^{\text{LDA}}) \nabla^2 u_\beta.$$
 (25)

The right-hand side of Eq. 23 can be calculated with the first-order perturbation theory by solving the Sternheimer equation for a perturbing potential whose spin- α and spin- β components are v_1 and v_2 , respectively.³³

Inserting Eqs. 21 and 22 into Eq. 15 and noting that u_{σ} equals $v_{\text{xcp},\sigma}$ at the convergence, we obtain the regularized OEP equation

$$\begin{bmatrix}
\frac{\delta(E_{xc} - E_{xc}^{\text{LDA}})}{\delta v_{s,\alpha}} + t_{\alpha} \\
\frac{\delta(E_{xc} - E_{xc}^{\text{LDA}})}{\delta v_{s,\beta}} + t_{\beta}
\end{bmatrix} = \left(\begin{bmatrix} X_{\alpha\alpha} & X_{\alpha\beta} \\ X_{\beta\alpha} & X_{\beta\beta} \end{bmatrix} + \begin{bmatrix} \frac{\lambda}{2} \nabla^2 & 0 \\ 0 & \frac{\lambda}{2} \nabla^2 \end{bmatrix}\right) \begin{bmatrix} v_{\text{xcp},\alpha} \\ v_{\text{xcp},\beta} \end{bmatrix}.$$
(26)

Compared to the original OEP equation 15, Eq. 26 is regularized by the additional Laplacian terms which increase as q^2 in the Fourier space and suppress the unphysical oscillations in $v_{\text{xcp},\sigma}$.

2.4 Analytical forces

Next, we derive the analytical forces for the total energy defined in Eq. 2. E depends on the atomic positions $\{\vec{R}_i\}$, the KS orbitals $\{\phi_{i\sigma}\}$, and the KS potential $v_{s,\sigma}$ (through E_p). In this work, Kleinman-Bylander norm-conserving potentials (NLPSs) are used. 34,35 $v_{s,\sigma}$ only contains the local potentials of these NLPSs and does not contain the nonlocal projectors. The analytical force for atom i is calculated as

$$\vec{F}_{i} = -\frac{dE}{d\vec{R}_{i}} = \vec{F}_{ia} + \vec{F}_{ib} + \vec{F}_{ic} \tag{27}$$

with the three components

$$\vec{F}_{ia} = -\sum_{\sigma} \int \frac{\partial E}{\partial v_{s,\sigma}(\vec{r})} \frac{dv_{s,\sigma}(\vec{r})}{d\vec{R}_i} dr^3$$
(28)

$$\vec{F}_{ib} = -\sum_{\sigma} \sum_{i} \int \frac{\delta E}{\delta \phi_{i\sigma}(\vec{r})} \frac{\partial \phi_{i\sigma}(\vec{r})}{\partial \vec{R}_{i}} dr^{3}$$
(29)

$$\vec{F}_{ic} = -\frac{\partial E}{\partial \vec{R}_i}. (30)$$

 \vec{F}_{ia} is due to the change of $v_{s,\sigma}$ with $\{\vec{R}_i\}$ fixed. Since $\partial E/\partial v_{s,\sigma}=0$ at convergence, we have $\vec{F}_{ia}=0$.

Next, we discuss \vec{F}_{ib} . When \vec{R}_i changes, both the local potential and the nonlocal projectors of atom i's NLPS change. In Eq. 29, $\partial \phi_{i\sigma}/\partial \vec{R}_i$ is calculated by only considering the change of atom i's nonlocal projectors, since the change of the local potential (contained in $v_{s,\sigma}$) has been considered when calculating \vec{F}_{ia} . $\partial \phi_{i\sigma}/\partial \vec{R}_i$ can be calculated by solving the Sternheimer equation for a variation of atom i's nonlocal projectors with the KS potential fixed. The term $\delta E/\delta \phi_{i\sigma}$ in Eq. 29 is calculated as

$$\frac{\delta E}{\delta \phi_{i\sigma}(\vec{r})} = \frac{\delta (T_s + J + E_{ext} + E_{nl} - TS)}{\delta \phi_{i\sigma}(\vec{r})} + \frac{\delta (E_{xc} + \lambda E_p)}{\delta \phi_{i\sigma}(\vec{r})},\tag{31}$$

in which the first part on the right-hand side is computed as

$$\frac{\delta(T_s + J + E_{ext} + E_{nl} - TS)}{\delta\phi_{i\sigma}} = f_{i\sigma}[\epsilon_{i\sigma} - (v_{xc,\sigma}^{\text{LDA}} + v_{xc,\sigma})]\phi_{i\sigma}, \tag{32}$$

where $\epsilon_{i\sigma}$ and $f_{i\sigma}$ are the eigenvalue and occupation number of the orbital i, respectively. In Eq. 31, $\delta E_{xc}/\delta \phi_{i\sigma}$ has already been calculated during the OEP calculations and can be directly used here to save the computational cost. $\delta E_p/\delta \phi_{i\sigma}$ in Eq. 31 is calculated as

$$\frac{\delta E_p}{\delta \phi_{i\sigma}(\vec{r})} = -\frac{1}{2} \sum_{\sigma'} \int \nabla^2 u_{\sigma'}(\vec{r}_1) \frac{\delta u_{\sigma'}(\vec{r}_1)}{\phi_{i\sigma}(\vec{r})} dr_1^3. \tag{33}$$

Since $v_{s,\sigma}$ is fixed for the calculation of \vec{F}_{ib} , the change of E_p is only due to the changes of the Hartree and the LDA XC potentials through $\phi_{i\sigma}$, and we have

$$\frac{\delta u_{\sigma'}(\vec{r}_1)}{\delta \phi_{i\sigma}(r)} = -\left[\frac{1}{|\vec{r} - \vec{r}_1|} + \delta(\vec{r} - \vec{r}_1)k_{\sigma'\sigma}^{\text{LDA}}(\vec{r})\right] f_{i\sigma}\phi_{i\sigma}(\vec{r}).$$
(34)

For \vec{F}_{ic} in Eq. 27, $\partial E/\partial \vec{R}_i$ is calculated by only considering the explicit dependence of

E on \vec{R}_i , which gives

$$\frac{\partial E}{\partial \vec{R}_i} = \frac{\partial (E_{ext} + E_{nl} + \lambda E_p)}{\partial \vec{R}_i},\tag{35}$$

where E_{nl} is the nonlocal pseudopotential energy due to the nonlocal projectors of the NLPSs. The last term above needs some special treatment. Note that E_p explicitly depends on \vec{R}_i through v_{ext} that consists of the local potentials of the NLPSs. By the chain rule, we have

$$\frac{\partial E_p}{\partial \vec{R}_i} = \int \frac{\partial E_p}{\partial v_{loc,i}(\vec{r}_1)} \frac{\partial v_{loc,i}(\vec{r}_1)}{\partial \vec{R}_i} dr_1^3, \tag{36}$$

where $v_{loc,i}$ is the local potential of atom i's NLPS. In this work, $\partial v_{loc,i}/\partial \vec{R}_i$ is calculated using the centered finite difference method by slightly displacing the atom i.

2.5 The flowchart of the self-consistent OEP calculations

The flowchart of our OEP scheme is similar to the conventional KS-DFT calculations. The major difference is that at each iteration a self-consistent KS-DFT-LDA calculation is performed with an additional external potential $v_{\text{xcp}}(\vec{r})$. The flowchart is given below.

- 1. Perform a self-consistent KS-DFT calculation with the Perdew-Burke-Ernzerhof (PBE) functional ³⁶ to obtain the initial guess for the KS orbitals, based on which we calculate $v_{\text{xcp}}(\vec{r})$ by solving the OEP equation 26.
- 2. Perform a self-consistent KS-DFT-LDA calculation with $v_{\text{xcp}}(\vec{r})$ being an additional external potential.
- 3. Based on the results from Step 2, obtain a new $v_{\text{xcp}}(\vec{r})$ by solving the OEP Eq. 26.
- 4. Check the convergence of $v_{\text{xcp}}(\vec{r})$. If it is not converged, go back to Step 2 for the next iteration.

The convergence of $v_{\text{xcp}}(\vec{r})$ can be accelerated by performing the Pulay mixing³⁷ at Step 3.

3 Numerical Details

Our new OEP scheme is implemented in the ABINIT program.³⁸ The OEP equation 26 is solved using the minimal residual method (MINRES) method.^{39–41} MINRES is not preconditioned in this work. When a reasonable regularization parameter is used, its convergence is fast. If the regularization parameter is very small, such as 10⁻⁶, the convergence becomes slow. The product between the KS linear response matrix and a vector is calculated by solving the Sternheimer equation.³³ NLPSs are used for all calculations. For N, C, O, Al, Si, Ga, As, and Cu, their NLPSs are generated using the FHI98pp program.⁴² For Ti, Fe, and Mn, the optimized norm-conserving Vanderbilt pseudopotentials are used,⁴³ which is more accurate due to the inclusion of the semicores. All the structures used in the OEP calculations are relaxed using the Vienna Ab initio Simulation Package (VASP) program.^{44–47}

The kinetic energy cutoffs for the calculations of N₂, Al bulk, Si bulk, CO/Cu(111), Fe bulk, GaAs, TiO₂, Mn₃O₄, and the isomerization reactions are 800 eV, 500 eV, 800 eV, 600 eV, 1200 eV, 800 eV, 800 eV, 800 eV, and 800 eV, respectively. The Fermi-Dirac smearing is used for all calculations. For Al bulk, Si bulk, CO/Cu(111), and Mn₃O₄ calculations, a smearing temperature of 0.1 eV is used. For TiO₂ and GaAs, a smearing temperature of 0.05 eV is used.

For Al bulk calculations, the Monkhorst-Pack k-point mesh ⁴⁸ of 8×8×8 is used for the face-centered cubic (FCC), body-centered cubic (BCC), cubic diamond (CD), and hexagonal close-packed (HCP) structures. For the simple cubic (SC) structure, a k-point mesh of $10\times10\times10$ is used. The unit cells contain 4, 2, 1, 2, and 4 atoms for FCC, BCC, SC, CD, and HCP structures, respectively. For Si bulk calculations, a k-point mesh of 8×8×8 is used for the CD, hexagonal diamond (HD), β -tin, body-centered-tetragonal 5 (bct5), SC, BCC, FCC, and HCP structures. A k-point mesh of 4×4×4 is used for the complex body-centered-cubic (BC8) structure. ^{49–51} Details about these silicon structures can be found in Ref. ^{52,53} The unit cells contain 2, 4, 8, 1, 2, 4, and 2 atoms for the CD, HD, BC8, β -tin, bct5, SC, HCP, FCC, and BCC structures, respectively. For TiO₂, the unit cells of anatase

and rutile both contain six atoms. A k-point mesh of $4\times4\times4$ is used for both anatase and rutile structures. For GaAs, a k-point mesh of $6\times6\times6$ is used for both zincblende and wurtzite structures. The unit cells contain two and four atoms for zincblende and wurtzite structures, respectively. For CO/Cu(111), the copper surface slab contains four layers, with a 2×2 surface. A k-point mesh of $4\times4\times1$ is used in all calculations. For Mn₃O₄, a k-point mesh of $3\times3\times3$ is used in all calculations. For BCC Fe, a k-point mesh of $6\times6\times6$ is used, and the unit cell contains two atoms.

4 Results and discussions

4.1 Convergence test

With the regularization, we can obtain well converged solutions to the OEP equation for a reasonable λ , which leads to good convergences for the DFT calculations. In Fig. 1, we show the convergences for three systems CO/Cu(111), BCC Fe, and Mn₃O₄. For Mn₃O₄, its ferromagnetic state is used. For all systems, the total energies converge to 10^{-4} eV within five iterations. The convergence of CO/Cu(111) is slower, which should be due to the difficulty of solving the OEP equation in the vacuum region. We address that, for all the systems without vacuum studied in this work, their convergences are as excellent as BCC Fe and Mn₃O₄.

The observed fast convergences are due to several reasons. First, a self-consistent KS-DFT-PBE calculation is performed at the start, which generates a good initial guess for the later OEP calculations. The second reason is that we only iterate v_{xcp} which is a small part of the KS potential. The last important reason is that, by iterating v_{xcp} , we avoid the "charge sloshing" problem caused by the Hartree potential. ^{46,54} As a result, there is no need to precondition the difference of v_{xcp} between successive iterations. Note that the charge sloshing problem still exists in the self-consistent KS-DFT-LDA calculations (Step 2 in the flowchart, Section 2.5).

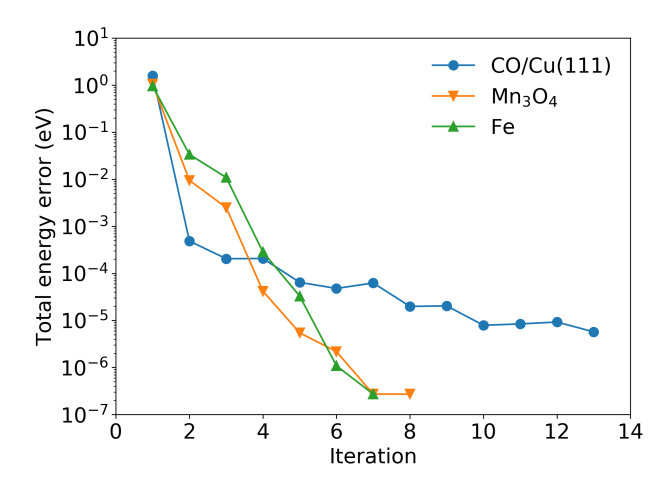


Figure 1: The convergences of the total energies for CO/Cu(111), Mn_3O_4 and BCC Fe, calculated with the regularization parameter $\lambda = 10^{-4}$.

4.2 Extrapolate energies to $\lambda = 0$

The energies at $\lambda=0$ can be estimated by extrapolating the energies based on Eqs. 12 and 13. As an example, the extrapolation for CD silicon is given in Fig. 2. E decreases faster as λ approaches zero, due to the fact that the slope $dE/d\lambda=E_p$ increases as λ decreases. This observation is consistent with Eq. 12. Similarly, E_{KS} also drops faster as λ increases, which is consistent with Eq. 13. Based on Eqs. 12 and 13, we extrapolate both E and E_{KS} to $\lambda=0$ and obtained similar parameters from the fittings: $\alpha=0.4624$, $c=2.54\times10^{-3}$, $E_0=-214.4761$ eV for E, and $\alpha=0.4033$, $c=4.51\times10^{-3}$, and $E_0=-214.4760$ eV for E_{KS} . Such similarities indicate that the asymptotic behaviors from Eqs. 12 and 13 are valid. Note that the obtained α are smaller than 1, which validates our previous assumption that the regularization term λE_p goes to zero as $\lambda \to 0$. Figure 2 also shows that, for a given λ , E_{KS} is much closer to the exact energy than E, which is due to the fact that E_{KS} is the first-order corrected energy (see Eq. 10).

4.3 Performance of the new regularization scheme

A key result in this work is the new regularization scheme defined in Eq. 4, which much reduces the magnitude of the regularization term and in turn reduces the impact of the

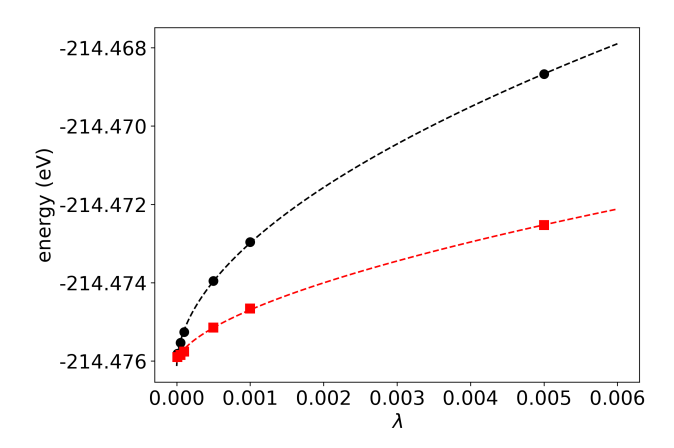


Figure 2: The extrapolation of the total energy E (black circles) and the first-order corrected energy E_{KS} (red squares) to $\lambda = 0$ for CD silicon. The data are fitted using Eqs. 12 and 13.

regularization on the total energy. In Fig. 3, the performance of the new scheme is compared against the old scheme (Eq. 3) for CD silicon at two regularization parameters $\lambda = 10^{-3}$ and $\lambda = 10^{-4}$. The error due to the regularization is defined as

$$E_{err} = E(\lambda) - E(\lambda = 0), \tag{37}$$

where $E(\lambda = 0)$ is obtained through the extrapolation. Fig. 3 shows that the new scheme reduces E_{err} by nearly one order of magnitude for both λ values. The reason is that we only regularize the difference between v_{xcp} and v_{xc}^{LDA} with the new scheme, while, with the old scheme, we regularize the fluctuations of v_{xcp} .

4.4 Forces

We now validate the analytical forces derived in Section 2.4. We evaluate the analytical forces at different bond lengths of N_2 and compare them against the benchmarks obtained using the centered finite difference method by displacing the atoms by ± 0.001 Å. The results are given in Table 1. A good agreement between the analytical forces and the benchmarks is observed.

In practice, we hope that forces do not depend much on the regularization parameter λ ,

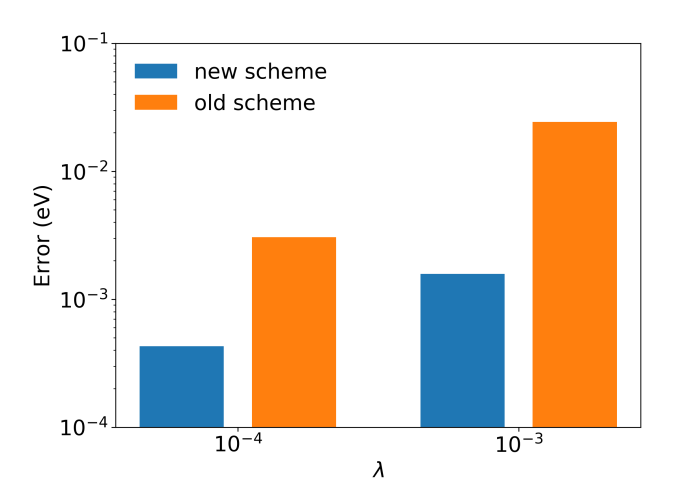


Figure 3: The energy errors per atom for CD silicon, calculated using the old (Eq. 3) and new (Eq. 4) regularization schemes.

Table 1: Forces (Ha/bohr) calculated using analytical $(F_{\rm analy})$ and finite-difference $(F_{\rm fd})$ methods at different bond lengths (a, Å) for N_2 , with $\lambda = 10^{-3}$.

\overline{a}	F_{analy}	$F_{ m fd}$
0.9	1.0702	1.0701
1.0	0.3409	0.3408
1.1	-0.0460	-0.0458
1.2	-0.2370	-0.2367
1.3	-0.3189	-0.3188
1.4	-0.3425	-0.3425

so that structural properties can be accurately obtained using a reasonable λ , without the extrapolation. In Table 2, we investigate the dependence of forces on λ . It is found that the forces are not sensitive to λ . This can be explained by Fig. 4, in which we plot total energy versus bond length for different λ values. The lower subplot gives the errors. The errors are uniform over a wide range of the bond length, which is the main reason why the forces are not sensitive to λ . Since the forces are insensitive to λ , we expect that structural properties are also insensitive to λ . This is confirmed in Table 3 which shows the structural properties of N₂, CD Si, Fe BCC, and rutile TiO₂ calculated for a wide range of λ . To calculate the bulk modulus of rutile TiO₂, its structure is first relaxed, and then the unit cell is uniformly scaled with the atoms' fractional coordinates fixed. For BCC Fe, we also find that the magnetic moment per atom is nearly unchanged (=2.94 μ_B) for all the λ values.

Table 2: The analytical forces (Ha/bohr) calculated for different bond lengths (a, Å) of N_2 .

		λ	
a	10^{-2}	10^{-3}	10^{-4}
0.9	1.0704	1.0702	1.0703
1.0	0.3408	0.3409	0.3408
1.1	-0.0460	-0.0460	-0.0460
1.2	-0.2371	-0.2370	-0.2369
1.3	-0.3189	-0.3189	-0.3188
1.4	-0.3424	-0.3425	-0.3425

Table 3: The equilibrium bond length b (Å) and the force constant k (N/m) of N₂, the equilibrium lattice constant a (Å) and bulk modulus B (GPa) of CD silicon and BCC Fe, and the equilibrium volume (Å³) and bulk modulus (GPa) of rutile TiO₂, calculated using different regularization parameters.

		$\overline{\mathrm{N}_{2}}$	S	i	F	e 'e	TiO	$\overline{O_2}$
λ	b	k	\overline{a}	В	\overline{a}	B	V_0	\overline{B}
10^{-2}	1.095	2300.50	5.444	96.1	2.928	139.7	61.801	309.2
10^{-3}	1.095	2300.63	5.444	96.2	2.927	139.3	61.660	312.0
10^{-4}	1.095	2300.59	5.444	96.2	2.928	139.3	61.660	312.0

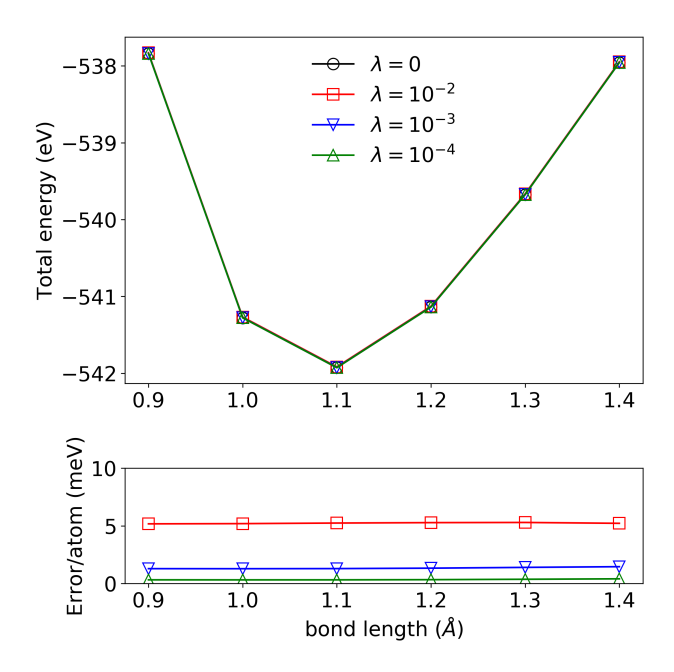


Figure 4: (Upper plot) Total energy versus the bond length for N₂, calculated using different regularization parameter λ . The energies extrapolated to $\lambda = 0$ are denoted as $\lambda = 0$. (Lower plot) The total energy error per atom $(E_{\lambda} - E_{\lambda=0})/2$.

4.5 Energy differences

One important task in practice is calculating the energy differences between systems. It is important that the energy differences are not sensitive to the regularization parameter λ , so that we do not need to extrapolate the results to $\lambda = 0$ in practice. In Table 4, we investigate the dependence of the energy differences on λ . All the energy differences are calculated based on E_{KS} , and the errors due to the regularization are defined as

$$E_{err,KS} = E_{KS}(\lambda) - E_{KS}(\lambda = 0). \tag{38}$$

For all examples, except CO/Cu(111), the benchmarks ($E_{KS}(\lambda = 0)$) are obtained by first extrapolating each system's energy to $\lambda = 0$, and then calculating the difference between the two extrapolated energies. For the CO/Cu(111) case, the benchmark is obtained by first extrapolating the top-site adsorption energy (E_{top}) and the hollow-site adsorption energy (E_{hollow}) to $\lambda = 0$ separately and then calculating the difference.

Table 4: Isomerization energies for the four reactions listed in Fig. 5. For Al, all energies (per atom) are referenced to FCC Al. For Si, all energies (per atom) are referenced to CD silicon. For TiO₂, the energy differences (per formula) between the rutile (rut) and anatase (ana) phases are listed. For GaAs, the energy differences (per formula) between the wurtzite (WZ) and zincblende (ZB) phases are listed. For CO/Cu(111), we list the adsorption energies at the top and hollow sites, and their differences. For Mn₃O₄, the energy differences (per formula) with respect to FiM6 are shown. The benchmarks ("extrap.") are obtained by extrapolating the energies to $\lambda = 0$ (see the text for details). All energies are in eV.

		λ		_			
	5×10^{-3}	10^{-3}	10^{-4}	extrap.			
	${\bf Isomerization}$						
reaction 1	-0.0721	-0.0722	-0.0722	-0.0722			
reaction 2	0.8475	0.8475	0.8476	0.8476			
reaction 3	0.7802	0.7796	0.7795	0.7795			
reaction 4	0.6196	0.6199	0.6199	0.6199			
	Al						
HCP	0.0458	0.0459	0.0459	0.0459			
BCC	0.1278	0.1278	0.1278	0.1279			
SC	0.4211	0.4212	0.4212	0.4210			
CD	0.8088	0.8089	0.8089	0.8090			
		30 0.0000 0.0000					
	Si						
HD	0.0130	0.0119	0.0114	0.0111			
BC8	0.1910	0.1899	0.1893	0.1891			
eta-tin	0.3825	0.3818	0.3814	0.3811			
$\cot 5$	0.4028	0.4024	0.4020	0.4015			
SC	0.5581	0.5577	0.5574	0.5569			
HCP	0.6408	0.6405	0.6402	0.6400			
FCC	0.6737	0.6734	0.6731	0.6729			
BCC	0.6844	0.6841	0.6839	0.6837			
		TiO),				
$E_{\rm rut} - E_{\rm ana}$	0.0746		0.0747	0.0747			
Ziut Zana	0.0.10	0.0121	0.0121	0.0121			
	GaAs						
$E_{\rm WZ} - E_{\rm ZB}$	0.0124	0.0124		0.0124			
	0.0121	0.0121	0.0121	0.0121			
	$\mathrm{CO}/\mathrm{Cu}(111)$						
$E_{ m top}$	0.8611	0.8624	0.8630	0.8632			
$E_{ m hollow}$	0.8234	0.8244	0.8249	0.8250			
$E_{\text{top}} - E_{\text{hollow}}$	0.0234 0.0378	0.0244 0.0380		0.0280 0.0382			
L'top L'hollow	0.0010	0.0000	0.0001	0.0002			
	${ m Mn_3O_4}$						
FiM1	0.0386	0.0378	0.0378	0.0379			
FiM2	0.0360 0.1167	0.0378 0.1160	0.0378 0.1159	0.0379 0.1160			
FiM3	0.1167 0.1364	0.1150 0.1358	0.1159 0.1357	0.1100 0.1357			
FiM4	0.1304 0.0292	0.1338 0.0293	0.1337 0.0294	0.1337 0.0295			
FiM5	0.0292 0.1433	0.0293 0.1426	0.0294 0.1425	0.0295 0.1425			
FM	0.1455 0.2243	0.1420	0.1425 0.2241	0.1425 0.2241			
Γ IVI	0.2243	$19^{0.2240}$	0.2241	0.2241			

We first examine the reaction energies of the isomerization reactions listed in Fig. 5. The agreement with the benchmark is excellent (on the order of 0.1 meV) for all reactions and for a wide range of λ . Such a good agreement is due to the good cancellation of $E_{err,KS}$ between the reactant and the product. Taking reaction 1 as an example, with $\lambda = 5 \times 10^{-3}$, $E_{err,KS}$ is 4.6 meV for the reactant and 4.8 meV for the product, which gives an error of about 0.2 meV for the reaction energy. All the good results obtained for the following examples are also due to the good cancellation of $E_{err,KS}$ between systems.

(1)
$$H_3C$$
— C $=$ CH \longrightarrow H_2C = C $=$ CH_2

(2) H_3C — C $=$ CH \longrightarrow H_2C $=$ CH_2

(3) H_3C \longrightarrow H_3C \longrightarrow

Figure 5: The four isomerization reactions used in this work. The reactions are drawn using the ChemSketch⁵⁵ program.

In Table 4, we calculate the energy differences between different Al bulk structures and FCC Al. Again, a good agreement with the benchmarks is observed. Particularly, we are able to well reproduce the small energy difference between the FCC and HCP structures.

Silicon is another good testbed, since many of its structures are close in energy. In Table 4, all the energies are referenced to CD silicon. A good agreement with the benchmarks is observed. Importantly, the new OEP method gives accurate energy differences between several structures that are close in energy, e.g., the energy difference between CD and HD, between β -tin and bct5, between HCP and FCC, and between FCC and BCC. In Table 4, we also examine the energy differences between TiO₂'s anatase and rutile phases and between GaAs's wurtzite and zincblende phases. Again, both energy differences are well reproduced.

We also examine CO's adsorption energies at the top and hollow sites of Cu(111). Both E_{top} and E_{hollow} converge quickly with respect to λ . Even with $\lambda = 5 \times 10^{-3}$, they differ from

the benchmarks by less than 2 meV. A more important quantity is the difference between E_{top} and E_{hollow} , which measures the relative stability of these two adsorption sites. We find that $(E_{\text{top}} - E_{\text{hollow}})$ converges even faster.

The last example in Table 4 is about the energy differences between different magnetic states of Mn_3O_4 . This is a challenging example, since the cancellation of $E_{err,KS}$ between different magnetic states may not be as good as the non-spin-polarized cases, due to the fact that the spin-up and spin-down electron numbers can be different for different magnetic states. Our calculations mainly follow Ref.,⁵⁶ and collinear spin-polarized calculations are performed for all systems. The structure of Mn_3O4 is shown in Fig. 6. In Table 4, FM denotes the ferromagnetic state and FiM denotes the ferrimagnetic state. The directions of the magnetic moments of the six Mn atoms (see Fig. 6) are $(\downarrow\downarrow\uparrow\uparrow\uparrow\uparrow\uparrow)$ for FiM1, $(\uparrow\uparrow\downarrow\uparrow\uparrow\uparrow\uparrow)$ for FiM2, $(\uparrow\uparrow\uparrow\downarrow\downarrow\uparrow\uparrow\uparrow)$ for FiM3, $(\uparrow\uparrow\uparrow\uparrow\downarrow\uparrow\uparrow\downarrow)$ for FiM4, $(\uparrow\uparrow\uparrow\uparrow\downarrow\uparrow\uparrow\uparrow)$ for FiM5, and $(\uparrow\downarrow\downarrow\uparrow\downarrow\uparrow\downarrow)$ for FiM6. All structures are fully relaxed with VASP using the LDA+U+J method⁵⁷ with U=4 eV and J=1.2 eV. In Table 4, all energies are referenced to FiM6 which has the lowest energy. It is encouraging to see that the errors are less than 1 meV for all magnetic states and for a wide range of λ . We are able to reproduce the small energy differences between these magnetic states that are close in energy, e.g., the energy difference (26 meV) between FiM2 and FiM5.

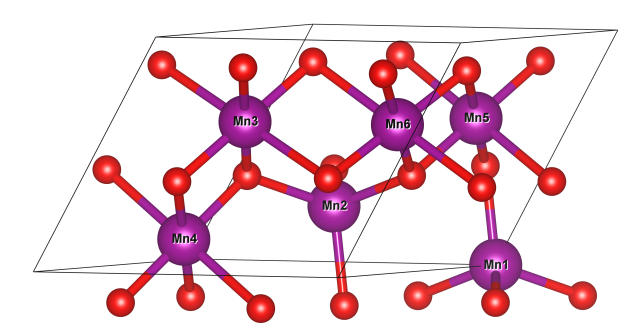


Figure 6: The unit cell for Mn₃O₄. Mn atoms are purple and oxygen atoms are red. To better illustrate the coordination of Mn atoms, the periodic images of some oxygen atoms are shown. The figure is made using the VESTA program.⁵⁸

5 Conclusions

In this work, we developed a new self-consistent OEP scheme that allows us to derive analytical forces based on the Hellmann-Feynman theorem. This is achieved by adding a regularization term that regularizes the XC potential to the total energy. In addition, we introduced a new regularization scheme to much reduce the impact of the regularization on DFT calculations. The key is to regularize the difference between the XC potential and an approximate XC potential, rather than regularizing the XC potential itself. The numerical results showed that forces and energy differences between systems are insensitive to a wide range of the regularization parameter. Therefore, many properties, such as ground-state structures, vibrational frequencies, and ground-state electronic states, can be calculated using a reasonable regularization parameter, without extrapolating the parameter to zero. This new OEP scheme is robust and nearly black-box (except for the regularization parameter). With increasing computer power, DFT calculations employing advanced, orbital-based XC functionals will become popular in the near future. We hope our method will facilitate these calculations, especially for applications where forces are required.

6 Acknowledgment

This work is supported by the National Science Foundation CAREER award (#1752769).

A A modified HSE06 functional

The short-range exact exchange (EXX) of the HSE06 functional is defined based on the EXX derived from the adiabatic connection fluctuation-dissipation theory (ACFDT).⁵⁹⁻⁶¹ The reason is that ACFDT-based EXX satisfies the sum rule of the exchange hole even for the cases where the KS orbitals are fractionally occupied.⁶² The short-range EXX is therefore

defined as

$$E_x^{SR} = -\frac{1}{2} \sum_{\sigma} \sum_{ij} f_{i\sigma} C_{ij,\sigma} \iint \frac{\operatorname{erfc}(\mu | \vec{r} - \vec{r}_1|)}{|\vec{r} - \vec{r}_1|} \times \phi_{i\sigma}(\vec{r}) \phi_{j\sigma}(\vec{r}_1) \phi_{i\sigma}(\vec{r}_1) \phi_{j\sigma}(\vec{r}) dr^3 dr_1^3$$
(39)

where $\mu = 0.2 \text{ Å}^{-1}$ and i and j loop over occupied orbitals. The original expression for $C_{ij,\sigma}$ is $C_{ij,\sigma} = 1 + \text{sign}(\epsilon_{i\sigma} - \epsilon_{j\sigma})$, where $\epsilon_{i\sigma}$ is the orbital i's eigenvalue. This expression causes problems for calculating $dE_x^{SR}/d\epsilon_{i\sigma}$ when $\epsilon_{i\sigma}$ and $\epsilon_{j\sigma}$ are identical. In this work, we modified $C_{ij,\sigma}$ by approximating the sign function with the tanh function, and the new expression is $C_{ij,\sigma} = 1 + \tanh(\gamma(\epsilon_{i\sigma} - \epsilon_{j\sigma}))$ with γ set to 100 atomic unit.

B Calculate $\delta E_{xc}/\delta v_{s,\sigma}$

 $E_x^{\rm SR}$ is a function of the occupation numbers, eigenvalues, and orbitals. The derivative is calculated as

$$\frac{\delta E_x^{\text{SR}}}{\delta v_{s,\sigma}(\vec{r})} = \sum_{\sigma'} \sum_{i} \frac{\partial E_x^{\text{SR}}}{\partial f_{i\sigma'}} \frac{\delta f_{i\sigma'}}{\delta v_{s,\sigma}(\vec{r})} + \sum_{i} \frac{\partial E_x^{\text{SR}}}{\partial \epsilon_{i\sigma}} \frac{\delta \epsilon_{i\sigma}}{\delta v_{s,\sigma}(\vec{r})} + \sum_{i} \int \frac{\delta E_x^{\text{SR}}}{\delta \phi_{i\sigma}(\vec{r}_1)} \frac{\delta \phi_{i\sigma}(\vec{r}_1)}{\delta v_{s,\sigma}(\vec{r})} dr_1^3.$$
(40)

The derivatives of $E_x^{\rm SR}$ with respect to $f_{i\sigma}$, $\epsilon_{i\sigma}$, and $\phi_{i\sigma}$ are straightforward. With the first-order perturbation theory, we have $\delta\epsilon_{i\sigma}/\delta v_{s,\sigma}(\vec{r}) = \phi_{i\sigma}(\vec{r})^2$. To calculate the last term in Eq. 40, we note $\delta\phi_{i\sigma}(\vec{r}_1)/\delta v_{s,\sigma}(\vec{r}) = G_{i\sigma}(\vec{r}_1,\vec{r})\phi_{i\sigma}(\vec{r})$, where $G_{i\sigma}$ is the KS Green's function. The last term of Eq. 40 then becomes

$$\sum_{i} \int \frac{\delta E_x^{\text{SR}}}{\delta \phi_{i\sigma}(\vec{r}_1)} G_{i\sigma}(\vec{r}_1, \vec{r}) \phi_{i\sigma}(\vec{r}) dr_1^3 = \sum_{i} \phi_{i\sigma}(\vec{r}) \psi_{i\sigma}(\vec{r})$$
(41)

where $\psi_{i\sigma}(\vec{r})$ is the orbital shift defined as

$$\psi_{i\sigma}(\vec{r}) = \int p(\vec{r}_1) G_{i\sigma}(\vec{r}_1, \vec{r}) dr_1^3 \tag{42}$$

with $p(\vec{r}) = \delta E_x^{\rm SR} / \delta \phi_{i\sigma}(\vec{r})$. $\psi_{i\sigma}(\vec{r})$ can be efficiently calculated using the equation

$$(\hat{H}_{\sigma} - \epsilon_{i\sigma}) |\psi_{i\sigma}\rangle = -(\hat{I} - |\phi_{i\sigma}\rangle \langle \phi_{i\sigma}|) |p\rangle, \qquad (43)$$

where \hat{H}_{σ} is the KS Hamiltonian of spin σ .

The other parts of the HSE06 functional are functionals that only depend on the electron density, and it is easy to calculate their derivatives. For example, the derivative of the long-range part of HSE06 is calculated as

$$\frac{\delta E_{xc}^{LR}}{\delta v_{s,\sigma}(\vec{r})} = \sum_{\sigma'} \int \frac{\delta E_{xc}^{LR}}{\delta \rho_{\sigma'}(\vec{r}_1)} \frac{\delta \rho_{\sigma'}(\vec{r}_1)}{\delta v_{s,\sigma}(\vec{r})} dr_1^3.$$
(44)

Note that $\delta \rho_{\sigma'}/\delta v_{s,\sigma}$ is the KS linear response, so the above integral can be calculated using the first-order perturbation theory. The calculation of $\delta E_{xc}^{\text{LDA}}/\delta v_{s,\sigma}$ in Eq. 14 follows the same route.

References

- (1) Hohenberg, P.; Kohn, W. Inhomogeneous electron gas. *Physical Review* **1964**, *136*, B864.
- (2) Kohn, W.; Sham, L. J. Self-consistent equations including exchange and correlation effects. *Physical Review* **1965**, *140*, A1133.
- (3) Kümmel, S.; Kronik, L. Orbital-dependent density functionals: Theory and applications. Reviews of Modern Physics 2008, 80, 3.

- (4) Casadei, M.; Ren, X.; Rinke, P.; Rubio, A.; Scheffler, M. Density-Functional Theory for f-Electron Systems: The α- γ Phase Transition in Cerium. Physical Review Letters 2012, 109, 146402.
- (5) Harl, J.; Schimka, L.; Kresse, G. Assessing the quality of the random phase approximation for lattice constants and atomization energies of solids. *Physical Review B* 2010, 81, 115126.
- (6) Olsen, T.; Thygesen, K. S. Random phase approximation applied to solids, molecules, and graphene-metal interfaces: From van der Waals to covalent bonding. *Physical Re-view B* 2013, 87.
- (7) Schimka, L.; Harl, J.; Stroppa, A.; Grüneis, A.; Marsman, M.; Mittendorfer, F.; Kresse, G. Accurate surface and adsorption energies from many-body perturbation theory. *Nature Materials* 2010, 9, 741–744.
- (8) Sharp, R.; Horton, G. A variational approach to the unipotential many-electron problem. *Physical Review* **1953**, *90*, 317.
- (9) Talman, J. D.; Shadwick, W. F. Optimized effective atomic central potential. *Physical Review A* **1976**, *14*, 36.
- (10) Sahni, V.; Gruenebaum, J.; Perdew, J. Study of the density-gradient expansion for the exchange energy. *Physical Review B* **1982**, *26*, 4371.
- (11) Görling, A.; Levy, M. Exact Kohn-Sham scheme based on perturbation theory. Physical Review A 1994, 50, 196–204.
- (12) Hirata, S.; Ivanov, S.; Grabowski, I.; Bartlett, R. J.; Burke, K.; Talman, J. D. Can optimized effective potentials be determined uniquely? The Journal of Chemical Physics 2001, 115, 1635–1649.

- (13) Ivanov, S.; Hirata, S.; Bartlett, R. J. Finite-basis-set optimized effective potential exchange-only method. *The Journal of Chemical Physics* **2002**, *116*, 1269–1276.
- (14) Yang, W.; Wu, Q. Direct Method for Optimized Effective Potentials in Density-Functional Theory. *Physical Review Letters* **2002**, *89*.
- (15) Wu, Q.; Cohen, A. J.; Yang, W. Analytic energy gradients of the optimized effective potential method. *The Journal of Chemical Physics* **2005**, *123*, 134111.
- (16) Payne, M. C.; Teter, M. P.; Allan, D. C.; Arias, T.; Joannopoulos, J. Iterative minimization techniques for ab initio total-energy calculations: molecular dynamics and conjugate gradients. *Reviews of modern physics* **1992**, *64*, 1045.
- (17) Krieger, J.; Li, Y.; Iafrate, G. Construction and application of an accurate local spin-polarized Kohn-Sham potential with integer discontinuity: Exchange-only theory. *Physical Review A* **1992**, *45*, 101.
- (18) Gritsenko, O. V.; Baerends, E. J. Orbital structure of the Kohn-Sham exchange potential and exchange kernel and the field-counteracting potential for molecules in an electric field. *Physical Review A* **2001**, *64*.
- (19) Sala, F. D.; Görling, A. Efficient localized Hartree–Fock methods as effective exact-exchange Kohn–Sham methods for molecules. *The Journal of Chemical Physics* **2001**, 115, 5718–5732.
- (20) Staroverov, V. N.; Scuseria, G. E.; Davidson, E. R. Effective local potentials for orbital-dependent density functionals. *The Journal of Chemical Physics* **2006**, *125*, 081104.
- (21) Heßelmann, A.; Götz, A. W.; Sala, F. D.; Görling, A. Numerically stable optimized effective potential method with balanced Gaussian basis sets. *The Journal of Chemical Physics* **2007**, *127*, 054102.

- (22) Thierbach, A.; Görling, A. Analytic energy gradients for the exact exchange Kohn-Sham method. *The Journal of Chemical Physics* **2020**, *152*, 114113.
- (23) Bleiziffer, P.; Heßelmann, A.; Görling, A. Efficient self-consistent treatment of electron correlation within the random phase approximation. *The Journal of chemical physics* **2013**, *139*, 084113.
- (24) Thierbach, A.; Görling, A. Analytic energy gradients for the self-consistent direct random phase approximation. *The Journal of Chemical Physics* **2020**, *153*, 134113.
- (25) Heaton-Burgess, T.; Bulat, F. A.; Yang, W. Optimized effective potentials in finite basis sets. *Physical Review Letters* **2007**, *98*, 256401.
- (26) Bulat, F. A.; Heaton-Burgess, T.; Cohen, A. J.; Yang, W. Optimized effective potentials from electron densities in finite basis sets. *The Journal of Chemical Physics* **2007**, *127*, 174101.
- (27) Huang, C. Analytical energy gradient for the embedded cluster density approximation.

 The Journal of Chemical Physics 2019, 151, 134101.
- (28) Perdew, J. P.; Wang, Y. Accurate and simple analytic representation of the electron-gas correlation energy. *Physical Review B* **1992**, *45*, 13244–13249.
- (29) Heyd, J.; Scuseria, G. E.; Ernzerhof, M. Hybrid functionals based on a screened Coulomb potential. *The Journal of Chemical Physics* **2003**, *118*, 8207–8215.
- (30) Heyd, J.; Scuseria, G. E. Efficient hybrid density functional calculations in solids: Assessment of the Heyd–Scuseria–Ernzerhof screened Coulomb hybrid functional. *The Journal of Chemical Physics* **2004**, *121*, 1187–1192.
- (31) Heyd, J.; Scuseria, G. E.; Ernzerhof, M. Erratum: "Hybrid functionals based on a screened Coulomb potential" [J. Chem. Phys. 118, 8207 (2003)]. The Journal of Chemical Physics 2006, 124, 219906.

- (32) Krukau, A. V.; Vydrov, O. A.; Izmaylov, A. F.; Scuseria, G. E. Influence of the exchange screening parameter on the performance of screened hybrid functionals. *The Journal of Chemical Physics* **2006**, *125*, 224106.
- (33) de Gironcoli, S. Lattice dynamics of metals from density-functional perturbation theory.

 Physical Review B 1995, 51, 6773–6776.
- (34) Hamann, D. R.; Schlüter, M.; Chiang, C. Norm-Conserving Pseudopotentials. *Physical Review Letters* **1979**, 43, 1494–1497.
- (35) Kleinman, L.; Bylander, D. M. Efficacious Form for Model Pseudopotentials. *Physical Review Letters* **1982**, 48, 1425–1428.
- (36) Perdew, J. P.; Burke, K.; Ernzerhof, M. Generalized Gradient Approximation Made Simple. *Physical Review Letters* **1996**, 77, 3865–3868.
- (37) Pulay, P. Convergence acceleration of iterative sequences. the case of scf iteration.

 Chem. Phys. Lett. 1980, 73, 393–398.
- (38) Gonze, X.; Amadon, B.; Anglade, P.-M.; Beuken, J.-M.; Bottin, F.; Boulanger, P.; Bruneval, F.; Caliste, D.; Caracas, R.; Côté, M., et al. ABINIT: First-principles approach to material and nanosystem properties. *Computer Physics Communications* **2009**, 180, 2582–2615.
- (39) Paige, C. C.; Saunders, M. A. Solution of Sparse Indefinite Systems of Linear Equations.

 SIAM Journal on Numerical Analysis 1975, 12, 617–629.
- (40) Choi, S.-C. T.; Paige, C. C.; Saunders, M. A. MINRES-QLP: A Krylov Subspace Method for Indefinite or Singular Symmetric Systems. SIAM Journal on Scientific Computing 2011, 33, 1810–1836.
- (41) Fong, D. C.-L.; Saunders, M. CG Versus MINRES: An Empirical Comparison. Sultan Qaboos University Journal for Science 2012, 16, 44.

- (42) Fuchs, M.; Scheffler, M. Ab initio pseudopotentials for electronic structure calculations of poly-atomic systems using density-functional theory. *Computer Physics Communications* **1999**, *119*, 67–98.
- (43) Hamann, D. R. Optimized norm-conserving Vanderbilt pseudopotentials. *Physical Review B* **2013**, 88.
- (44) Kresse, G.; Hafner, J. Ab initio molecular dynamics for liquid metals. *Physical Review B* 1993, 47, 558–561.
- (45) Kresse, G.; Furthmüller, J. Efficiency of ab-initio total energy calculations for metals and semiconductors using a plane-wave basis set. *Computational Materials Science* 1996, 6, 15–50.
- (46) Kresse, G.; Furthmüller, J. Efficient iterative schemes for ab initio total-energy calculations using a plane-wave basis set. *Physical Review B* **1996**, *54*, 11169–11186.
- (47) Kresse, G.; Joubert, D. From ultrasoft pseudopotentials to the projector augmentedwave method. *Physical Review B* **1999**, *59*, 1758–1775.
- (48) Monkhorst, H. J.; Pack, J. D. Special points for Brillouin-zone integrations. *Physical Review B* **1976**, *13*, 5188–5192.
- (49) Wentorf, R. H.; Kasper, J. S. Two New Forms of Silicon. *Science* **1963**, 139, 338–339.
- (50) Joannopoulos, J. D.; Cohen, M. L. Electronic Properties of Complex Crystalline and Amorphous Phases of Ge and Si. I. Density of States and Band Structures. *Physical Review B* 1973, 7, 2644–2657.
- (51) Crain, J.; Clark, S. J.; Ackland, G. J.; Payne, M. C.; Milman, V.; Hatton, P. D.; Reid, B. J. Theoretical study of high-density phases of covalent semiconductors. I. Ab initio treatment. *Physical Review B* 1994, 49, 5329-5340.

- (52) Zhou, B.; Wang, Y. A.; Carter, E. A. Transferable local pseudopotentials derived via inversion of the Kohn-Sham equations in a bulk environment. *Physical Review B* **2004**, 69.
- (53) Huang, C.; Carter, E. A. Transferable local pseudopotentials for magnesium, aluminum and silicon. *Physical Chemistry Chemical Physics* **2008**, *10*, 7109.
- (54) Kerker, G. P. Efficient iteration scheme for self-consistent pseudopotential calculations.

 Physical Review B 1981, 23, 3082–3084.
- (55) ChemSketch, Advanced Chemistry Development Inc, Toronto, Canada, version 2021.2.1.
- (56) Lim, J. S.; Saldana-Greco, D.; Rappe, A. M. Improved pseudopotential transferability for magnetic and electronic properties of binary manganese oxides from DFT+U+J calculationsImproved pseudopotential transferability for magnetic and electronic properties of binary manganese oxides from DFT+U+J calculations. *Physical Review B* **2016**, *94*.
- (57) Liechtenstein, A. I.; Anisimov, V. I.; Zaanen, J. Density-functional theory and strong interactions: Orbital ordering in Mott-Hubbard insulators. *Physical Review B* 1995, 52, R5467–R5470.
- (58) Momma, K.; Izumi, F. VESTA 3for three-dimensional visualization of crystal, volumetric and morphology data. *Journal of Applied Crystallography* **2011**, *44*, 1272–1276.
- (59) Langreth, D. C.; Perdew, J. P. The exchange-correlation energy of a metallic surface.

 Solid State Communications 1975, 17, 1425–1429.
- (60) Gunnarsson, O.; Lundqvist, B. I. Exchange and correlation in atoms, molecules, and solids by the spin-density-functional formalism. *Phys. Rev. B* **1976**, *13*, 4274–4298.

- (61) Langreth, D. C.; Perdew, J. P. Exchange-correlation energy of a metallic surface wave-vector analysis. *Physical Review B* **1977**, *15*, 2884.
- (62) Yan, Z.; Perdew, J. P.; Kurth, S. Density functional for short-range correlation: Accuracy of the random-phase approximation for isoelectronic energy changes. *Physical Review B* 2000, 61, 16430.

TOC Graphic

